Journal of Inorganic Biochemistry 199 (2019) 110797

Contents lists available at ScienceDirect

Journal of Inorganic Biochemistry

journal homepage: www.elsevier.com/locate/jinorgbio

Implications of structural heterogeneity for the electronic structure of the final oxygen-evolving intermediate in photosystem II

Vera Krewald[a], Frank Neese[b], Dimitrios A. Pantazis[b,*]

[a] Theoretische Chemie, Fachbereich Chemie, Technische Universität Darmstadt, Alarich-Weiss-Str. 4, 64287 Darmstadt, Germany
[b] Max-Planck-Institut für Kohlenforschung, Kaiser-Wilhelm-Platz 1, 45470 Mülheim an der Ruhr, Germany

A B S T R A C T

Heterogeneity in intermediate catalytic states of the oxygen-evolving complex (OEC) of Photosystem II is known from a wide range of experimental and theoretical data, but its potential implications for the mechanism of water oxidation remain unexplored. We delineate the consequences of structural heterogeneity for the final step of the catalytic cycle by tracing the evolution of three spectroscopically relevant and structurally distinct components of the last metastable S_3 state to the transient O_2-evolving S_4 state of the OEC. Using quantum chemical calculations, we show that each S_3 isomer leads to a different electronic structure formulation for the active S_4 state. Crucially, in addition to previously hypothesized Mn(IV)-oxyl species, we establish for the first time, how a genuine Mn(V)-oxo can be obtained in the catalytically active S_4 state: this takes the form of a five-coordinate and locally high-spin ($S_{Mn} = 1$) Mn(V) site. This formulation for the S_4 state evolves naturally from a preceding S_3-state structural intermediate that contains a quasi-trigonal-bipyramidal Mn(IV) ion. The results strongly suggest that water binding in the S_3 state is not prerequisite for reaching the oxygen-evolving S_4 state of the complex, supporting the notion that both substrates are preloaded at the beginning of the catalytic cycle. This scenario allows true four-electron metal-centered hole accumulation to precede O—O bond formation and hence the latter can proceed via a genuine even-electron mechanism. This can occur as intramolecular nucleophilic coupling of two oxo units synchronously with the binding of a water substrate for the next catalytic cycle.

1. Introduction

Light-driven water oxidation in nature is accomplished by photosystem II, a membrane-embedded multi-subunit enzyme that employs an oxo-bridged Mn_4Ca cluster to accumulate four oxidizing equivalents and catalyze the formation of dioxygen [1–9]. The Mn_4CaO_x cluster of the oxygen-evolving complex (OEC) passes through five metastable storage states S_i (i = 0–4), of which S_4, the state that has accumulated four oxidizing equivalents, is the final and as yet unobserved transient state that evolves dioxygen (Fig. 1). Long-standing debates about the mechanistic details of O—O bond formation have centered on the nature of the active Mn-oxygen species, for example oxo versus oxyl, the sequence of electron and proton transfers, and the type of the critical coupling step, i.e. radical coupling or nucleophilic attack. Numerous hypotheses have been proposed and some of them have been explored computationally [9–23]. However, no consensus can be reached in the absence of experimental information on active intermediate(s) and, in view of the accumulated uncertainties, regarding the identity of substrates.

The constantly improving understanding of the lower S_0, S_1, and S_2 states has contributed significantly to the refinement of possible structural models. Atomic-resolution crystallographic data of the dark-stable S_1 state have been instrumental in this effort [24,25], particularly from studies that employ X-ray free electron laser (XFEL) sources to control radiation damage [26]. The S_2 state is commonly accepted to consist of two interconvertible $Mn(IV)_3Mn(III)$ valence isomers [27,28] with distinct bonding topology and spectroscopic properties [29–40]. At present, the research frontier does not extend beyond the last metastable state of the catalytic cycle, the S_3 state, in which it is most commonly accepted that all four Mn ions of the OEC are present as Mn(IV) [41–47]. Rationalizing diverse experimental data on the S_3 state in terms of precise atomistic models is complicated by the fact that spectroscopy reveals the coexistence of multiple forms [40,47–52]. Preliminary attempts at structural characterization of the S_3 state with XFEL crystallography [53–56] have not proven to be sufficiently illuminating because they are mutually incompatible and lead to drastically diverging interpretations. As discussed recently [57], currently available crystallographic models suffer from issues relating to state quantification, information content, data analysis [58], and discrimination of structural heterogeneity [9,57]. Most importantly, the proposed structurally ambiguous models are difficult, if not impossible, to reconcile with the concrete spectroscopic information on the electronic structure of the Mn ions of the cluster [42,47]. In a separate development, however, the rich and state-specific information from various types of spectroscopy has formed the basis for refinement of possible spectroscopy-consistent atomistic models for the S_3 state using

* Corresponding author.
E-mail address: dimitrios.pantazis@kofo.mpg.de (D.A. Pantazis).

https://doi.org/10.1016/j.jinorgbio.2019.110797
Received 14 June 2019; Received in revised form 18 July 2019; Accepted 1 August 2019
Available online 01 August 2019
0162-0134/

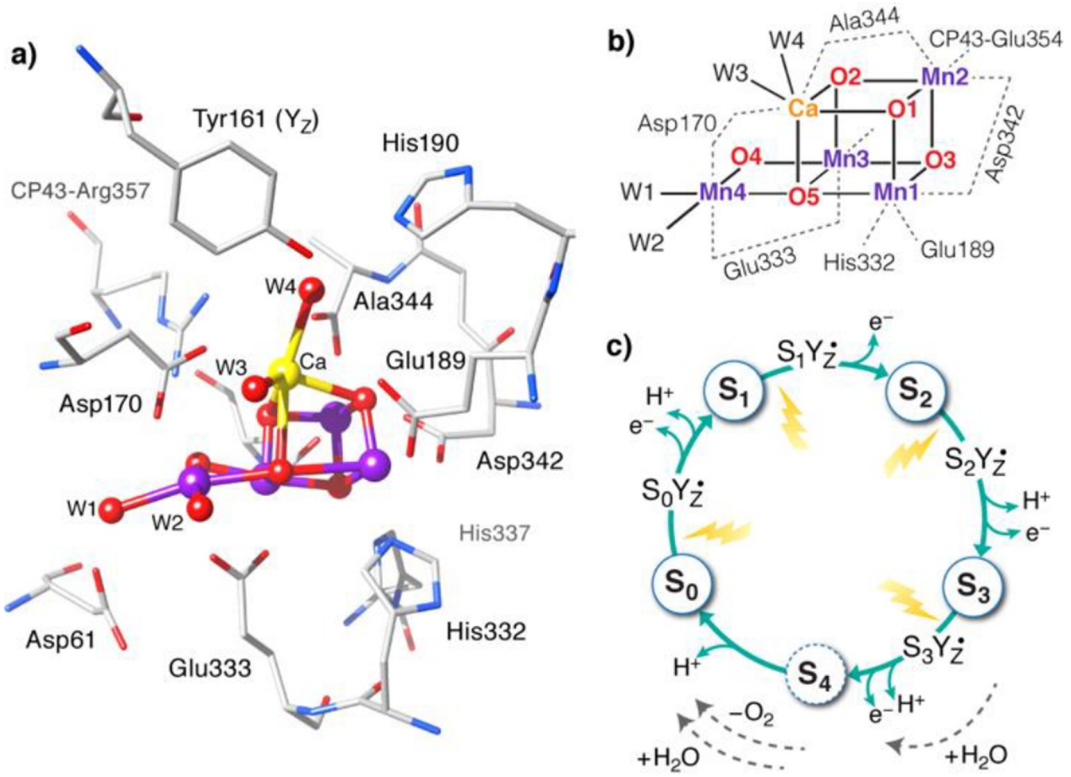

Fig. 1. a) XFEL crystallographic structure of the S_1 state of the OEC [26]. b) Schematic depiction of the OEC with labeling of core atoms and the first coordination sphere amino acids. c) The five-state cycle of water oxidation.

modern quantum chemical approaches.

Computational modelling of structural intermediates in the S_2–S_3 transition and their correlation with spectroscopic observations provided evidence for three distinct but functionally connected structural forms of a $Mn(IV)_4$ cluster in the S_3 state [59–61]. Alternative conceivable valence-isomeric forms [62–65] that involve "early onset" O—O bond formation [57] are not obviously compatible with the spectroscopy of the S_3 state or the kinetics of substrate exchange and will not be considered in the present study. The two known components of the S_2 state, shown in Fig. 2, differ in the location of the unique Mn (III) ion and the bonding between the centrally located O5 bridge and the terminal Mn1 and Mn4 ions. The cluster thus exists as either an "open cubane" with spin $S = 1/2$ (model $\mathbf{S_2}^{\mathbf{A}}$ in Fig. 2), or as a "closed cubane" with spin $S \geq 5/2$ ($\mathbf{S_2}^{\mathbf{B}}$). The first one corresponds to the multiline $g = 2$ EPR signal of the S_2 state, the latter to the $g = 4.1$ (or higher [38,39]) signal. Given that the S_2–S_3 transition involves oxidation and deprotonation as well as potentially the coordination of a water molecule, at least three structural models can be immediately conceived and have been described for the S_3 state [59] as depicted in Fig. 2: (i) $\mathbf{S_3}^{\mathbf{B}}$, a model containing a five-coordinate, approximately trigonal-bipyramidal Mn(IV) attached to a Mn_3CaO_4 cubane [59]; (ii) $\mathbf{S_3}^{\mathbf{B,W}}$, a closed cubane model that can be generated by low-barrier water binding at the Mn4 ion of $\mathbf{S_3}^{\mathbf{B}}$ [59] (or alternatively by direct OH binding at the internal site of Mn4) [28]; and (iii) $\mathbf{S_3}^{\mathbf{A,W}}$ [45,66] with four six-coordinate Mn(IV) resulting from internal rearrangement [60,61] of $\mathbf{S_3}^{\mathbf{B,W}}$ (or alternatively by direct OH binding to the internal coordination site of Mn1 in the $\mathbf{S_2}^{\mathbf{A}}$ form) [66,67]. In the present nomenclature, the superscript W indicates that a new water is bound to a manganese ion.

The trigonal bipyramidal $\mathbf{S_3}^{\mathbf{B}}$ was shown by Retegan et al. to be a requisite component of the S_3 state because analysis of the S_2–S_3 transition established that only the $\mathbf{S_2}^{\mathbf{B}}$ component of the S_2 state can proceed to S_3 [59]. This is in agreement with EPR studies which showed that only the minority $g = 4.1$ component of the S_2 state progresses to S_3 [48]. Therefore, cofactor oxidation in the S_2–S_3 transition requires deprotonation of a terminal water ligand but *not* water binding [59]. The $\mathbf{S_3}^{\mathbf{B}}$ structure was shown to provide a straightforward explanation for the near-infrared (NIR) absorption in the S_3 state and of the resulting tyrosyl radical split EPR signal [59]. The $\mathbf{S_3}^{\mathbf{A,W}}$ component was identified by magnetic resonance studies [47,68] and supported by simulations of EXAFS spectra [69,70]. $\mathbf{S_3}^{\mathbf{B,W}}$ is required to connect the other two [60]. In the sequence presented in Fig. 2, water binding occurs in $\mathbf{S_3}^{\mathbf{B}}$ at the position previously occupied by W1 through a water channel terminating at Mn4 [59], which is also associated with substrate analogue delivery to the OEC [71–73]. Importantly, the three forms are interconvertible regardless of the details of water binding and of the S_2–S_3 transition, and hence all three are plausible components of the "S_3 state". Therefore, as the equilibrium remains experimentally undefined, it is necessary to consider equally all interconvertible S_3 components as candidates for advancement to the S_4 state.

The implications of the structural heterogeneity in the S_3 state for the chemical nature of the catalytically active S_4 state have not been explored, given that only the $\mathbf{S_3}^{\mathbf{A,W}}$ model of Fig. 2 has been considered in past studies. In the present work, we trace the progression of each S_3 state component computationally and construct appropriate models for the resulting S_4 "hot" species. A novel, five-coordinate Mn(V)-oxo intermediate is identified, which uniquely supports the scenario of exclusively metal-based storage of the four oxidizing equivalents before initiation of O—O bond formation.

2. Methodology

2.1. Structural models

The S_4 state models contain the Mn_4Ca cluster with all oxo bridges and three or four additional H_2O, OH or terminal O ligands bound to Mn1 and Mn4 to complete the ligand sphere of Mn1 (octahedral) and Mn4 (octahedral or trigonal-bipyramidal). Two water molecules are

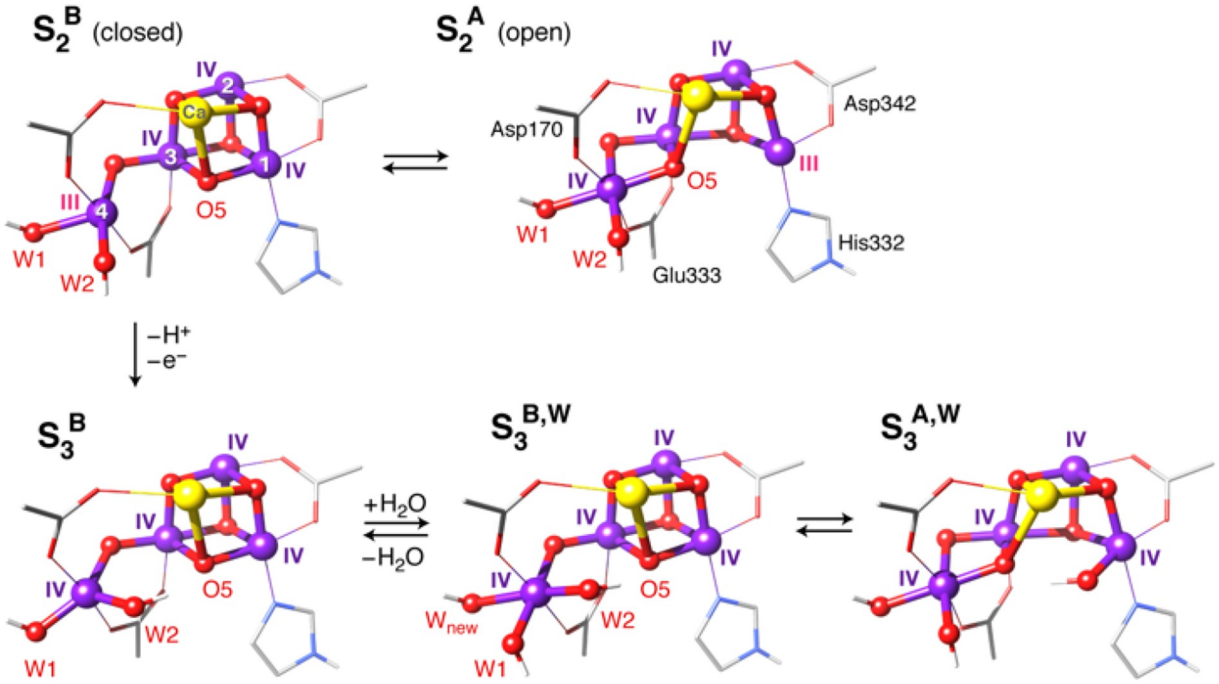

Fig. 2. Models of the OEC core for the S_2 and S_3 states [59], indicating a likely progression sequence and the structural relationships between different components. For clarity, only four amino acid residues are depicted.

bound to Ca^{2+}, and six or seven additional water molecules are placed at crystallographic positions. All amino acid residues directly bound to Mn and Ca (from the D1 protein unless stated otherwise) are included: His332, Glu189, Asp342, Ala344, CP43-Glu354, Asp170, Glu333. Furthermore, Tyr161 (Y_Z), His190, His337 (H-bond with O3), CP43-Arg357 and backbones of Leu343, Ser169 and part of Gly171 are included. It is noted that inclusion of the redox-active Tyr161 and its His190 partner is essential for any studies of S-state transitions in the OEC; omission of these residues can lead to serious artifacts and errors in both, electronic structure and computed relative energetics of intermediates. The total size of the models was 223 atoms. Quantum cluster models of this size were shown to yield results and properties indistinguishable from size-converged quantum-mechanics/molecular-mechanics (QM/MM) calculations [74].

2.2. Geometry optimizations

All calculations were carried out with ORCA [75]. Geometry optimizations of the S_4 state models and calculations of electronic structure properties and energetics used the TPSSh hybrid-meta-GGA density functional [76], making use of the resolution-of-the-identity and the chain-of-spheres approximations (RIJCOSX) [77] with increased integration grids (Grid6 and GridX6 in ORCA convention). The choice of this specific functional, which incorporates a moderate percentage of Hartree–Fock exchange (10%), was motivated by numerous past studies that supported its reliable performance for geometries and energetics of transition metal complexes in general [78–80], as well as of redox potentials [81], spin states, and various spin-dependent spectroscopic properties of exchange-coupled manganese complexes in particular [82–86]. It is noted that TPSSh was recently shown to even surpass “double-hybrid” functionals for exchange-coupled manganese systems [87]. Scalar relativistic effects were incorporated through the zero-order regular approximation (ZORA) [88–90] applying the one-center approximation. Relativistically recontracted [91] versions of the Karlsruhe polarized triple-ζ basis sets [92] were used for all atoms except for carbons and hydrogens, for which the double-ζ polarized versions were employed. Weigend's auxiliary basis sets [93] were used in fully decontracted form. Dispersion effects were taken into account with Grimme's D3 corrections using the Becke–Johnson damping function [94,95]. Normal optimization criteria for geometry convergence and tight convergence criteria for the SCF procedure were applied. The electrostatic and structural effects of the protein were considered implicitly through the COSMO solvation model [96] with a dielectric constant of 8 and by placing constraints on specific backbone carbon and associated hydrogen atoms as described in detail previously [45].

2.3. Calculations of X-ray absorption spectra

The X-ray absorption spectra were predicted with time-dependent density functional theory calculations (TD-DFT) using the TPSSh density functional with the same RIJCOSX approximation as above, using Grid6 and GridX6 as well as an integration accuracy of 6.0 in ORCA nomenclature. The ZORA Hamiltonian was used with the ZORA-recontracted def2-TZVP(-f) basis sets [97] on all atoms except C and H, for which ZORA-def2-SVP was used. The XAS spectra for each Mn ion were predicted with 80 roots and their intensities summed up to yield the total spectrum for each OEC model [98]. The spectra are shifted to higher energies by 36.3 eV as specified in benchmark studies [99].

3. Results and discussion

3.1. Geometric and electronic structures of S_4 state intermediates

Upon oxidation of the S_3 state, an intermediate $S_3Y_Z\cdot$ state is formed. The precise chemical details of this intermediate remain under investigation [100–102], but it is established that $S_3Y_Z\cdot$ is subsequently deprotonated in a kinetically resolvable step [103,104], leading to the reduction of the $Y_Z\cdot$ radical with concomitant oxidation of the manganese cluster. In the S_2 and $S_2Y_Z\cdot$ states, the most acidic proton is part of W1 in the open cubane $\mathbf{S_2^A}$, oriented towards Asp61, a residue associated with proton removal from the OEC [59]. Any other deprotonation step is disfavored by at least 10 kcal/mol [59]. This finding is not surprising since W1 is the only Mn-bound H_2O, and the resulting species

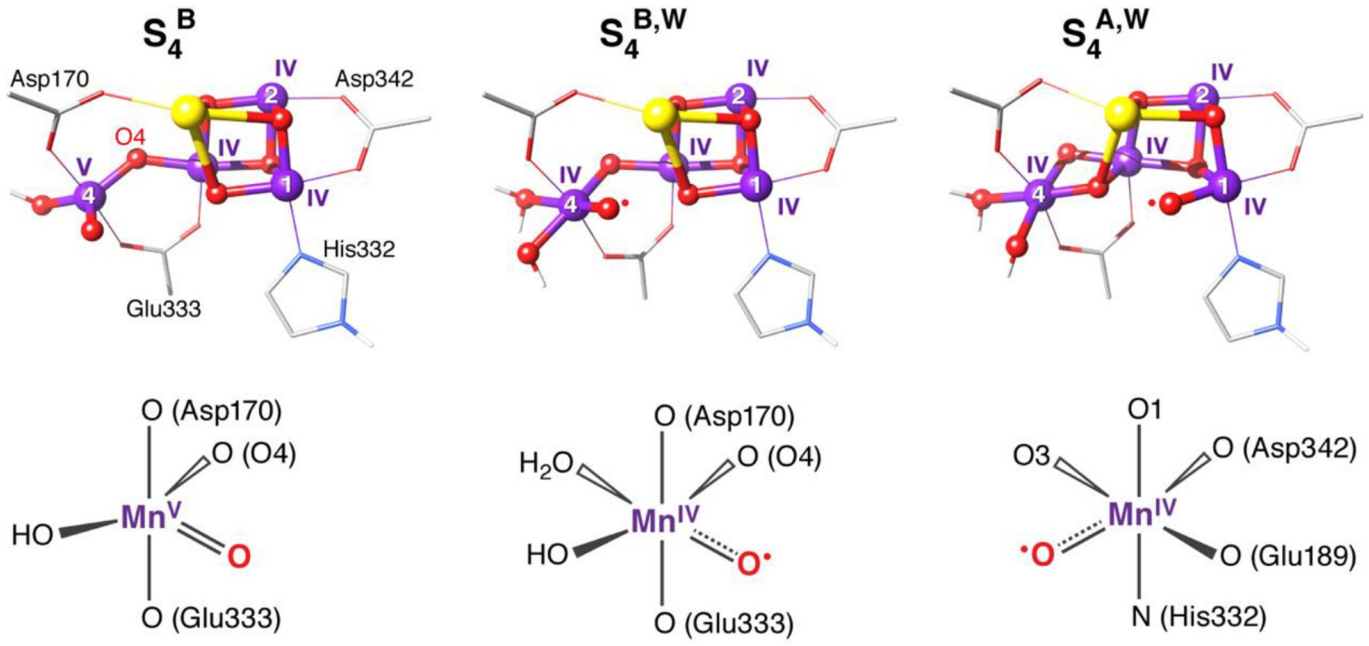

Fig. 3. The three lowest-energy forms of the OEC cluster in the S_4 state, as derived from deprotonation and oxidation of the three distinct S_3-state models. $\mathbf{S_4}^{\mathbf{B}}$ contains a five-coordinate locally high-spin Mn(V)-oxo site, whereas the other models have Mn(IV)-oxyl units at the Mn4 or Mn1 ions of the cluster.

benefits from better stabilization than the deprotonation product of the closed-cubane form.

Applying similar considerations to the S_3-state models presented in Fig. 2, the most acidic protons in $\mathbf{S_3}^{\mathbf{A,W}}$ and $\mathbf{S_3}^{\mathbf{B,W}}$ are on W_{new} (H_2O), the only doubly protonated water ligand, and either of the hydroxyl ligands W1 or W2 in $\mathbf{S_3}^{\mathbf{B}}$. Experiments have shown that substrates cannot exchange anymore after $S_3Y_Z\cdot$ is formed [105], which is strongly indicative of both substrates being fully deprotonated. Deprotonation of a water group in $\mathbf{S_3}^{\mathbf{A,W}}/\mathbf{S_3}^{\mathbf{B,W}}$ is thus disfavored, as it requires proton transfer from one hydroxo ligand (on Mn1 or Mn4) to the deprotonated W_{new} on Mn4. We have nevertheless considered all of the above deprotonation pathways and their subsequent oxidation to the S_4 state. The three S_4 state models shown in Fig. 3 are the most likely outcomes. Higher-energy alternatives including higher and lower overall multiplicities are discussed in the Supporting Information.

Models $\mathbf{S_4}^{\mathbf{A,W}}$ and $\mathbf{S_4}^{\mathbf{B,W}}$ contain Mn(IV)-oxyl units [106,107], similar to structures studied previously in the computational literature [18,20,108]. The former is an open-cubane structure with the oxyl group attached to Mn1, while the latter is a closed-cubane structure with the oxyl group *trans* to W1 at the octahedrally coordinated Mn4. In $\mathbf{S_4}^{\mathbf{A,W}}$, the Mulliken spin population of Mn1 is 2.76 with −0.51 on the oxyl, and similarly for $\mathbf{S_4}^{\mathbf{B,W}}$, the spin populations on the atoms of the Mn-O· unit are 2.48 and –0.43. The other manganese ions have spin populations of 2.89 or higher, and oxo-bridge spin populations are negligible (< 0.10). Therefore, all manganese ions in these two structures have a formal d^3 high-spin configuration typical of Mn(IV) (see Scheme 1 for an idealized diagram). $\mathbf{S_4}^{\mathbf{A,W}}$ is 9.4 kcal/mol lower in energy than $\mathbf{S_4}^{\mathbf{B,W}}$. The greater stability of the Mn(IV)-oxyl on the Mn1 site rather than the Mn4 site is consistent with earlier reports [19]. Mn(V)-oxo forms of $\mathbf{S_4}^{\mathbf{B,W}}$ were found to be > 13 kcal/mol higher in energy than $\mathbf{S_4}^{\mathbf{A,W}}$ (see Supporting Information for several additional higher-energy models). The present calculations thus agree with previous studies, concluding that six-coordinate Mn ions in the S_4 state of the OEC preferably form Mn(IV)-oxyl over low-spin Mn(V)-oxo species.

In contrast, a genuine Mn(V)-oxo is found in the S_4 state model $\mathbf{S_4}^{\mathbf{B}}$ that contains a five-coordinate, approximately trigonal-bipyramidal Mn4 ion. At this center, the in-plane coordinating ligands are the oxo unit (derived from W2), a hydroxyl ligand (W1) and the mono-μ-oxo bridge to the closed $Mn(IV)_3CaO_4$ cubane, while the axial ligands are the carboxylate groups of Asp170 and Glu333. The Mulliken spin populations are 1.84 for Mn(V), 0.14 for the attached oxo, and 2.91–2.94 for the remaining Mn(IV) ions, leaving no doubt that $\mathbf{S_4}^{\mathbf{B}}$ contains a d^2 high-spin Mn(V)-oxo entity (Scheme 1). The alternative closed-shell singlet configuration for this Mn(V)-oxo species is 6.6 kcal/mol higher in energy.

Although $\mathbf{S_4}^{\mathbf{B}}$ is not isodesmic with $\mathbf{S_4}^{\mathbf{A,W}}$ and $\mathbf{S_4}^{\mathbf{B,W}}$, complicating the discussion of relative energies, a reasonable approximation was made by positioning the unbound water molecule in the second coordination sphere. This led to $\mathbf{S_4}^{\mathbf{B}}$ being only 3.7 kcal/mol higher in energy than $\mathbf{S_4}^{\mathbf{A,W}}$, an energy difference smaller than the strength of a weak O−H hydrogen bond (4–8 kcal/mol) [109]. Therefore, within the uncertainties of the method, the two models cannot be considered energetically distinguishable. A synthetic example of a mononuclear five-coordinate Mn(V)-oxo complex has been reported by Borovik and coworkers [110,111]. It uses the tripodal ligand H_3buea^{3-} which leads to an axial positioning of the oxo ligand. The Mn−O bond length is 1.68 Å (determined from EXAFS and DFT) [110] longer than that found in $\mathbf{S_4}^{\mathbf{B}}$ (1.61 Å) where the oxo is found in the equatorial position of the approximately trigonal-bipyramidal Mn4 site. This difference in the coordination sphere is presumably the reason why the Borovik complex has significant spin density on the oxo (0.45 by EPR; 0.41 by DFT) [110], whereas in $\mathbf{S_4}^{\mathbf{B}}$ the equatorially positioned oxo does not.

In conclusion, $\mathbf{S_4}^{\mathbf{B}}$ represents a plausible candidate for the fully oxidized catalytic species in natural water oxidation, supporting a novel formulation for the S_4 state as a five-coordinate Mn(V)-oxo species. Critical for the atomic-level formulation of the catalytic cycle is the conclusion that from the electronic structure point of view water binding during the S_2–S_3 transition or in the S_3 state is not required for progression to the S_4 state.

3.2. Spectroscopic differentiation of S_4 state intermediates

Before discussing possible mechanistic implications of the above results, it is interesting to ask how one could spectroscopically differentiate between Mn-oxo and Mn-oxyl forms in the transient S_4 species, under the assumption that spectroscopic observation of S_4 intermediates might be achievable in the future. First of all, if either $\mathbf{S_4}^{\mathbf{A,W}}$ or $\mathbf{S_4}^{\mathbf{B,W}}$ represent the true S_4 state, the significant spin density on the oxyl

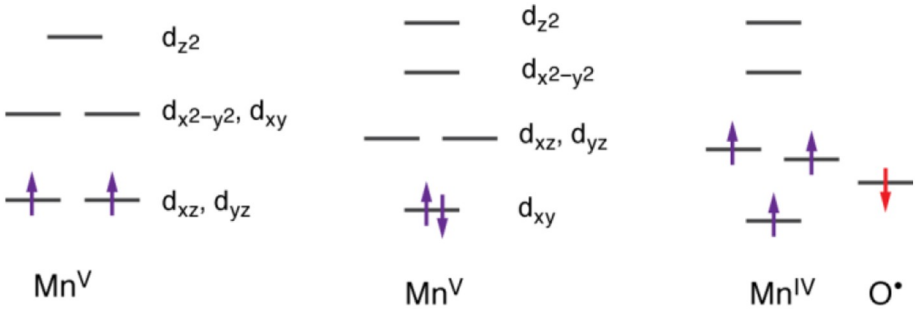

Scheme 1. Orbital splitting diagrams and electron configurations for a high-spin Mn(V) ion in a trigonal bipyramidal field relevant for $\mathbf{S_4}^{\mathbf{B}}$ (left), a tetragonal field that promotes a low-spin Mn(V) configuration (center) and the energetically more favorable Mn(IV)–oxyl situation that describes models $\mathbf{S_4}^{\mathbf{B,W}}$ and $\mathbf{S_4}^{\mathbf{A,W}}$ (right).

radical could be detectable by EPR techniques that probe ligand hyperfine couplings such as ^{17}O ENDOR. The absence of significant O-based spin in $\mathbf{S_4}^{\mathbf{B}}$ impedes detection by EPR, and the absence of an oxygen-centered radical signal would likely not be considered satisfactory evidence to prove the presence of a genuine Mn(V)-oxo entity. However, in view of recent advances in protein X-ray spectroscopy, we suggest that the K pre-edge signatures of transient species might be considered as a more direct way to discriminate between the proposed models.

A time-resolved Mn K_α fluorescence study identified a kinetically resolved intermediate in the $S_3Y_Z^•$ to S_0Y_Z transition that corresponds to a deprotonated $S_3Y_Z^•$ species, i.e. the Mn oxidation states remain the same as in S_3 [104,112]. Because the fourth oxidation equivalent has not yet been transferred from the tyrosine to the manganese-calcium cluster, a further intermediate in which the Mn_4CaO_x cluster is oxidized (the S_4 state) must follow this species, but this remained unresolved [113]. Here we sought to assess whether the K pre-edges of $\mathbf{S_4}^{\mathbf{A,W}}$, $\mathbf{S_4}^{\mathbf{B,W}}$ and $\mathbf{S_4}^{\mathbf{B}}$ would be sufficiently distinct to permit differentiation. These features are computed with time-dependent density functional theory, which has been shown to predict Mn K pre-edge spectra in good agreement with experiment [45,98,99,114,115].

K pre-edge transitions of transition metal complexes formally arise from electric quadrupole-allowed 1s to 3d transitions. Deviations from centrosymmetry allow inherently more intense electric dipole-allowed transitions due to admixture of p-character into the metal-d-dominated orbitals. Similarly, a weakening of the Mn—O bond due to a strong ligand *trans* to the oxo group is expected to lower the pre-edge intensity [116]. In the case of a trigonal-bipyramidal Mn(V)-oxo compared with an octahedrally coordinated Mn(IV)-oxyl, the former is expected to have a stronger, shorter bond with increased p/d-mixing, and to deviate more significantly from centrosymmetry, and should thus have a higher pre-edge intensity [110,116–119]. This is indeed observed in the calculated K pre-edge spectra (see Fig. 4). The intensity predicted for the Mn(V)-oxo $\mathbf{S_4}^{\mathbf{B}}$ is significantly higher than that predicted for the Mn (IV)-oxyl models $\mathbf{S_4}^{\mathbf{A,W}}$ and $\mathbf{S_4}^{\mathbf{B,W}}$. From the analysis of the contributions of excitations originating from the individual Mn ions, the increased total intensity of $\mathbf{S_4}^{\mathbf{B}}$ is clearly attributable to the penta-coordinate Mn4 ion (see the Supporting Information for individual contributions). Owing to the same Mn oxidation state, the Mn(IV)-oxyl models of the S_4 state have similar pre-edge intensities as the corresponding precursor S_3 models. This is mirroring previous observations in a synthetic complex [120]. Given that the $\mathbf{S_3}^{\mathbf{A,W}}$ pre-edge corresponds well with the experimental spectrum for the S_3 state [45], we suggest that a significant rise in intensity could be the tell-tale signature for the formation of the five-coordinate $\mathbf{S_4}^{\mathbf{B}}$ Mn(V)-oxo species in the S_4 state.

3.3. Implications for the mechanism of water oxidation

In the following, we will explore the implications of the above results for the mechanism of O—O bond formation. First of all, it is stressed that all three possible components of the S_3 state support cofactor oxidation to the S_4 state. This is not an inescapable result and alternative outcomes in terms of the calculations would be formation of radical species in the periphery of the model, for example in aromatic residues; this is not observed here. In the case of the $\mathbf{S_3}^{\mathbf{B}}$ structure, the remarkable result that oxidation remains metal-centered demonstrates that water binding is not prerequisite for oxidative advancement to the S_4 state. Although water can bind to the $\mathbf{S_3}^{\mathbf{B}}$ intermediate from the Asp61-terminating water channel at Mn4 [8,59,71,72], this process has a low barrier and is reversible [59]. Whereas the more stable species $\mathbf{S_3}^{\mathbf{A,W}}$ has been most easily identified by EPR spectroscopy [47], substrate deprotonation might be inhibited in this model (in analogy to the situation in the $S_2Y_Z^•$ intermediates [59]), thus preventing catalytic advancement. This would mean that water binding in S_3 might not be productive. Importantly, the water that can be associated with the OEC in the S_3 state would not be a substrate in the running catalytic cycle. This in turn implies that both substrate waters are already present in the $\mathbf{S_3}^{\mathbf{B}}$ intermediate and hence that both substrate waters are preloaded at the starting point of the cycle, the S_0 state.

The two types of electronic structure represented by the Mn(IV)-oxyl $\mathbf{S_4}^{\mathbf{A,W}}$/$\mathbf{S_4}^{\mathbf{B,W}}$ and the Mn(V)-oxo $\mathbf{S_4}^{\mathbf{B}}$ lead to fundamentally distinct scenarios for catalytic progression. In the former, *three* metal-centered oxidations (S_0–S_3) are followed by one ligand-centered oxidation, i.e. the last light-driven electron transfer implicates directly the substrate, necessitating subsequent radical-type chemistry. In contrast, in the case of $\mathbf{S_4}^{\mathbf{B}}$ all light-driven oxidation events in the Kok cycle are metal-centered. Therefore, formation of the five-coordinate Mn(V)-oxo is the only way in which *four* oxidizing equivalents can be stored in the Mn ions of the OEC prior to initiation of water oxidation. This distinction is not merely conceptual but has direct relevance for understanding the principles of biological water oxidation. Detailed thermodynamic considerations have shown that a concerted four-electron oxidation of water is thermodynamically most favorable, followed by two two-electron transfers, while odd-electron transfer sequences represent the thermodynamically least favorable scenarios [121]. The formation of a Mn(IV)-oxyl species in the S_4 state is part of an odd-electron transfer sequence and hence belongs to the thermodynamically unfavorable category. Conversely, progressing through the five-coordinate Mn(V)-oxo unit of the $\mathbf{S_4}^{\mathbf{B}}$ model, all charge accumulation steps including formation of the S_4 state are metal-based as required for genuine even-electron (concerted four-electron or sequential 2 + 2 electron) oxidation of substrates.

It is common in discussions of alternative hypothetical mechanisms for biological water oxidation to refer to the conflicting views of radical-based versus nucleophilic attack mechanisms. However, this is somewhat misleading because such discussions tend to describe competing mechanisms that – in the context of biological water oxidation – are not equally supported by actual quantum chemical studies. An overview of quantum chemical studies that utilize realistic models of the OEC and report on their electronic structure (for representative cases see [17–20]) reveals that regardless of the nomenclature used to

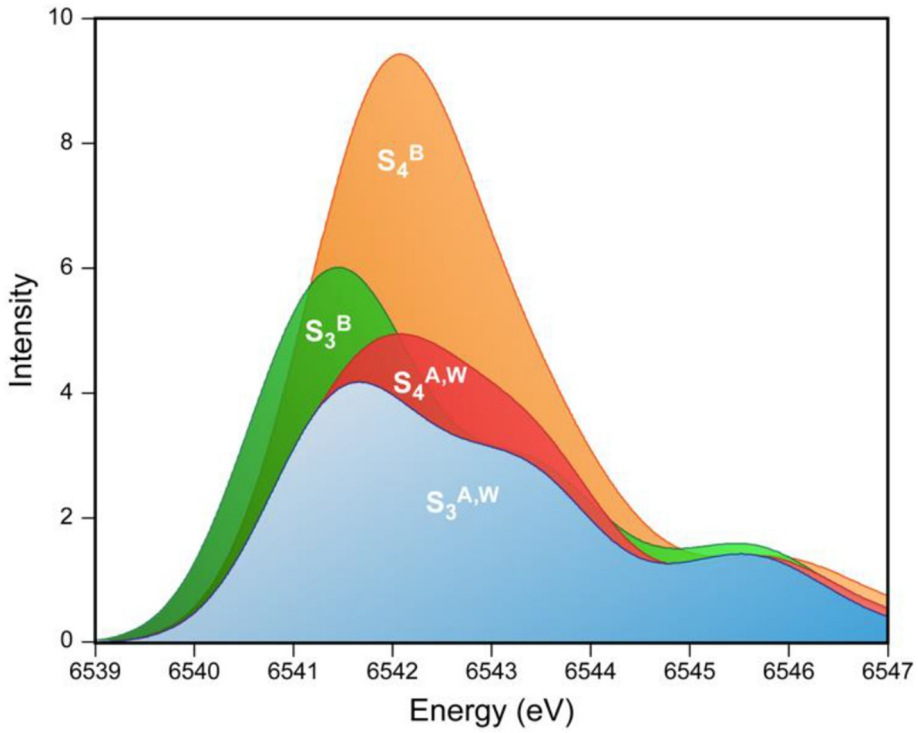

Fig. 4. Comparison of computed Mn K pre-edge absorption spectra for the Mn(IV)-oxyl species $\mathbf{S_4}^{\mathbf{A,W}}$ (red) and its precursor $\mathbf{S_3}^{\mathbf{A,W}}$ (blue), and for the Mn(V)-oxo species $\mathbf{S_4}^{\mathbf{B}}$ (orange) and its precursor $\mathbf{S_3}^{\mathbf{B}}$ (green).

describe the O—O bond formation process, "radical coupling", "oxo–oxyl coupling" or "nucleophilic attack", computational studies always find a Mn(IV)-oxyl in the S_4 state as the lowest-energy electronic configuration. To our knowledge, no quantum chemical study of realistic OEC models has identified a bona fide Mn(V)-oxo species that would support a genuine, rather than nominal, nucleophilic O—O coupling scenario. Here "genuine" refers to the demonstrated absence of radical character for both O atoms that form the O—O bond. The present results confirm that obtaining a Mn(IV)-oxyl species is the inescapable result of constraining the Mn center to be six-coordinate, the common assumption of previous computational studies. In contrast, the electronic structure of the five-coordinate $\mathbf{S_4}^{\mathbf{B}}$ is the first genuine Mn(V) species and, in terms of physiological catalytic progression, comes about by simply delaying water binding at this site in the S_3–S_4 transition. In turn, this species provides a quantum chemical basis for even-electron chemistry in the OEC.

O—O bond formation based on oxyl-containing species such as $\mathbf{S_4}^{\mathbf{A,W}}$ has been extensively discussed in past studies and will not be further elaborated here. Of more interest is the question what alternative mechanistic possibilities become possible based on the novel $\mathbf{S_4}^{\mathbf{B}}$ model. In this case at least two distinct ways of forming the O—O bond can be envisaged. First, the terminal oxo group of Mn4 can be attacked by any vicinal nucleophilic water. Ca-bound H_2O (or OH) is an obvious candidate. However, experiment indicates that substrate exchange rates are similar in S_2 and S_3 [122] while differing significantly in lower S-state intermediates, and that substrate exchange is arrested before the S_4 state [105]. Assigning either of the Ca-bound H_2O molecules – which probably retain their protonation states at least until the S_3 state [59] – as substrate would be hard to reconcile with the above observations. In addition, there is strong spectroscopic evidence in support of O5 being one of the substrates [73].

Although the involvement of a Ca-bound species cannot be conclusively excluded, we favor instead an alternative scenario in which the O—O bond is formed between the μ_3-oxo bridge bound to Ca, Mn1 and Mn3, and the terminal oxo of five-coordinate Mn4(V). This scenario tentatively identifies the substrates with the W2 and O5 oxygen atoms of the lower S-states. The nucleophilic coupling between the terminal Mn4 oxo and O5 entirely avoids protonated intermediates and is expected to involve a minimal amount of reorganization energy, as the two groups are ideally positioned to react. Mechanistic details will be examined in depth in future studies, but Fig. 5 shows how an electron rearrangement might occur. The proposed mechanism for O—O bond formation could be quasi-synchronous and would involve redistribution of four electrons: Mn1 and Mn3 would be reduced by one electron each from Mn(IV) to Mn(III), while Mn4 would be reduced by two electrons from Mn(V) to Mn(III). Therefore, the OEC could transition from the S_4 state (with Mn oxidation states IV-IV-IV-V) to the S_0 state (III-IV-III-III), avoiding intermediates with metal oxidation states that would implicate peroxidic species.

The high-spin electronic configuration of the five-coordinate Mn4(V) in $\mathbf{S_4}^{\mathbf{B}}$ is expected to enable unimpeded same-spin electron transfer to the unoccupied Mn4 d orbitals for a direct high-spin d^2 to high-spin d^4 reduction, which would not be the case for an octahedral closed-shell Mn(V) ion (Scheme 1). O—O bond formation could be coupled with water binding externally at Mn4, along the incipiently formed Jahn–Teller axis of this ion. Another water could be delivered directly at the site of the departing O_2 [123] to form the O5 bridge of the subsequent S_0 state [124]. Note that in the above scenario depicted in Fig. 5 the newly formed dioxygen moiety would find itself located at the locus of three converging Jahn–Teller axes (of Mn1, Mn3, and Mn4). This is likely a critical contributor to the driving force for the expulsion of O_2 from the metal cavity and potentially a factor that determines the strict irreversibility of oxygen evolution in the OEC.

4. Conclusions

In the present work we examined if and how each of three possible structural models for the last metastable S_3 state of the oxygen-evolving complex may progress by deprotonation and oxidation to the transient oxygen-evolving S_4 state. Our results demonstrate that water binding in the S_3 state is not required for progression to the S_4 state, and hence on electronic structure grounds both substrate waters can already be

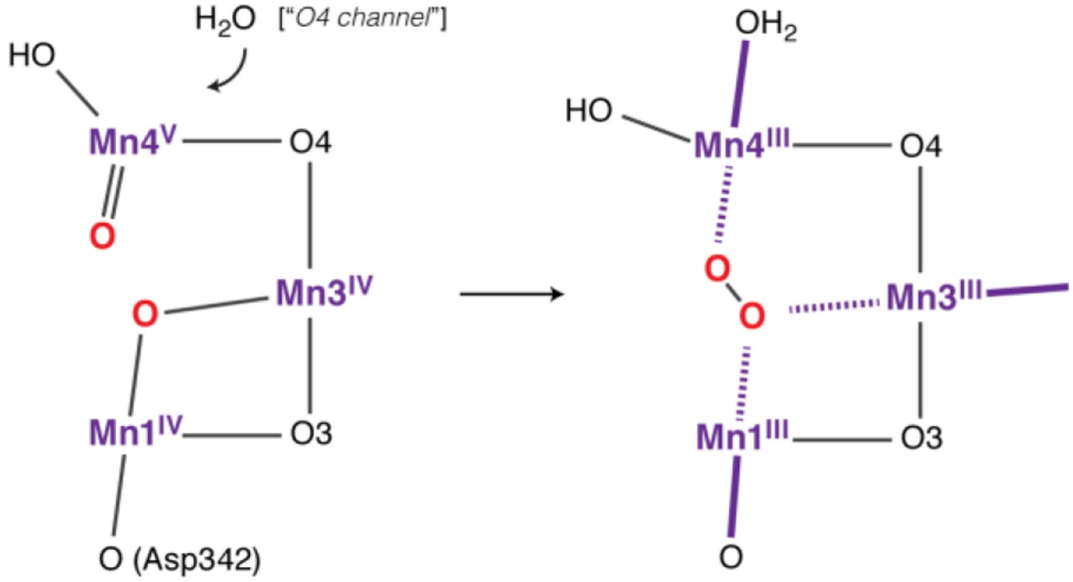

Fig. 5. Proposed O—O intramolecular nucleophilic coupling mechanism based on the Mn4(V)-oxo species $\mathbf{S_4^B}$. Redistribution of four electrons can be accompanied by concerted water binding at the Mn4 ion. In terms of redox state, the cluster transitions from S_4 (IV-IV-IV-V) to S_0 (III-IV-III-III) with the O_2 placed at the locus of three Jahn–Teller axes (indicated by thick and dashed lines).

bound upon reconstitution of the S_0 state. It is confirmed that structures where all Mn ions are six-coordinate invariably lead to a terminal Mn (IV)-oxyl species in the S_4 state. By contrast, Mn-based oxidation in the S_3–S_4 transition is possible for a structural form of S_3 that contains a five-coordinate Mn(IV) ion. Upon advancement to the S_4 state this structure yields an unprecedented formulation for the final catalytic state: an energetically favorable species that contains a five-coordinate Mn(V)-oxo center. The Mn(V) ion in this case has a local high-spin electronic configuration and the oxo unit has no radical character. The S_4 structural model with the five-coordinate site is therefore the only one that allows a genuine Mn(V)-oxo species to form in the OEC. The model drastically departs from the commonly accepted progression of three metal-based and one ligand-based light-driven oxidations (the only computationally supported scenario until now), since it allows for complete separation between a charging phase of the cycle, in which four holes are stored on the Mn ions, and the catalytic phase of di-oxygen evolution. As a consequence, this intermediate opens the possibility of genuine even-electron water oxidation chemistry. This potentially allows the realization of the thermodynamically most favorable scenario of four-electron chemistry. Based on this model it is suggested that the initial O—O bond formation step can be a genuine intramolecular nucleophilic coupling with concerted water binding. As opposed to previously proposed mechanisms, the present suggestion does not need to invoke oxygen radical intermediates in O—O bond formation, or indeed at any point in the catalytic cycle of biological water oxidation.

Acknowledgements

We thank the Max Planck Society for financial support. This research made use of the Balena High Performance Computing (HPC) Service at the University of Bath.

Appendix A. Supplementary data

Supplementary data to this article can be found online at https://doi.org/10.1016/j.jinorgbio.2019.110797.

References

[1] R.E. Blankenship, Molecular Mechanisms of Photosynthesis, 2nd edn, Wiley, Chichester, 2014.
[2] J.P. McEvoy, G.W. Brudvig, Chem. Rev. 106 (2006) 4455–4483.
[3] J. Messinger, G. Renger, Chapter 17 photosynthetic water splitting, Primary Processes of Photosynthesis, Part 2: Principles and Apparatus, vol. 9, The Royal Society of Chemistry, Cambridge, 2008, pp. 291–349.
[4] H. Dau, I. Zaharieva, Acc. Chem. Res. 42 (2009) 1861–1870.
[5] N. Cox, D.A. Pantazis, F. Neese, W. Lubitz, Acc. Chem. Res. 46 (2013) 1588–1596.
[6] V. Krewald, M. Retegan, D.A. Pantazis, Top. Curr. Chem. 371 (2016) 23–48.
[7] M. Pérez-Navarro, F. Neese, W. Lubitz, D.A. Pantazis, N. Cox, Curr. Opin. Chem. Biol. 31 (2016) 113–119.
[8] M. Askerka, G.W. Brudvig, V.S. Batista, Acc. Chem. Res. 50 (2017) 41–48.
[9] D.A. Pantazis, ACS Catal. 8 (2018) 9477–9507.
[10] V.L. Pecoraro, M.J. Baldwin, M.T. Caudle, W.-Y. Hsieh, N.A. Law, Pure Appl. Chem. 70 (1998) 925–929.
[11] J.S. Vrettos, J. Limburg, G.W. Brudvig, Biochim. Biophys. Acta Bioenerg. 1503 (2001) 229–245.
[12] J.P. McEvoy, G.W. Brudvig, Phys. Chem. Chem. Phys. 6 (2004) 4754–4763.
[13] J. Messinger, Phys. Chem. Chem. Phys. 6 (2004) 4764–4771.
[14] T.A. Betley, Y. Surendranath, M.V. Childress, G.E. Alliger, R. Fu, C.C. Cummins, D.G. Nocera, Philosophical Transactions of the Royal Society B: Biological Sciences 363 (2008) 1293–1303.
[15] E.M. Sproviero, J.A. Gascon, J.P. McEvoy, G.W. Brudvig, V.S. Batista, Coord. Chem. Rev. 252 (2008) 395–415.
[16] P.E.M. Siegbahn, Acc. Chem. Res. 42 (2009) 1871–1880.
[17] E.M. Sproviero, J.A. Gascon, J.P. McEvoy, G.W. Brudvig, V.S. Batista, J. Am. Chem. Soc. 130 (2008) 3428–3442.
[18] P.E.M. Siegbahn, Biochim. Biophys. Acta Bioenerg. 1827 (2013) 1003–1019.
[19] X. Li, P.E.M. Siegbahn, Phys. Chem. Chem. Phys. 17 (2015) 12168–12174.
[20] Y. Guo, H. Li, L.-L. He, D.-X. Zhao, L.-D. Gong, Z.-Z. Yang, Phys. Chem. Chem. Phys. 19 (2017) 13909–13923.
[21] B. Zhang, L. Sun, Dalton Trans. 47 (2018) 14381–14387.
[22] K. Yamaguchi, M. Shoji, H. Isobe, S. Yamanaka, T. Kawakami, S. Yamada, M. Katouda, T. Nakajima, Mol. Phys. 116 (2018) 717–745.
[23] M. Shoji, H. Isobe, Y. Shigeta, T. Nakajima, K. Yamaguchi, Chem. Phys. Lett. 698 (2018) 138–146.
[24] Y. Umena, K. Kawakami, J.-R. Shen, N. Kamiya, Nature 473 (2011) 55–60.
[25] A. Tanaka, Y. Fukushima, N. Kamiya, J. Am. Chem. Soc. 139 (2017) 1718–1721.
[26] M. Suga, F. Akita, K. Hirata, G. Ueno, H. Murakami, Y. Nakajima, T. Shimizu, K. Yamashita, M. Yamamoto, H. Ago, J.-R. Shen, Nature 517 (2015) 99–103.
[27] D.A. Pantazis, W. Ames, N. Cox, W. Lubitz, F. Neese, Angew. Chem. Int. Ed. 51 (2012) 9935–9940.
[28] D. Bovi, D. Narzi, L. Guidoni, Angew. Chem. Int. Ed. 52 (2013) 11744–11749.
[29] G.C. Dismukes, Y. Siderer, Proc. Natl. Acad. Sci. U. S. A. 78 (1981) 274–278.
[30] J.L. Casey, K. Sauer, Biochim. Biophys. Acta Bioenerg. 767 (1984) 21–28.
[31] J.C. De Paula, G.W. Brudvig, J. Am. Chem. Soc. 107 (1985) 2643–2648.
[32] J.L. Zimmermann, A.W. Rutherford, Biochim. Biophys. Acta Bioenerg. 767 (1984) 160–167.
[33] J.L. Zimmermann, A.W. Rutherford, Biochemistry 25 (1986) 4609–4615.
[34] J.C. de Paula, W.F. Beck, A.-F. Miller, R.B. Wilson, G.W. Brudvig, J. Chem. Soc. Faraday Trans. 83 (1987) 3635–3651.
[35] J. Cole, V.K. Yachandra, R.D. Guiles, A.E. McDermott, R.D. Britt, S.L. Dexheimer, K. Sauer, M.P. Klein, Biochim. Biophys. Acta Bioenerg. 890 (1987) 395–398.

[36] D.H. Kim, R.D. Britt, M.P. Klein, K. Sauer, J. Am. Chem. Soc. 112 (1990) 9389–9391.
[37] A. Boussac, J.-J. Girerd, A.W. Rutherford, Biochemistry 35 (1996) 6984–6989.
[38] O. Horner, E. Rivière, G. Blondin, S. Un, A.W. Rutherford, J.-J. Girerd, A. Boussac, J. Am. Chem. Soc. 120 (1998) 7924–7928.
[39] A. Boussac, A.W. Rutherford, Biochim. Biophys. Acta Bioenerg. 1457 (2000) 145–156.
[40] A. Boussac, I. Ugur, A. Marion, M. Sugiura, V.R.I. Kaila, A.W. Rutherford, Biochim. Biophys. Acta Bioenerg. 1859 (2018) 342–356.
[41] M. Haumann, C. Müller, P. Liebisch, L. Iuzzolino, J. Dittmer, M. Grabolle, T. Neisius, W. Meyer-Klaucke, H. Dau, Biochemistry 44 (2005) 1894–1908.
[42] I. Zaharieva, P. Chernev, G. Berggren, M. Anderlund, S. Styring, H. Dau, M. Haumann, Biochemistry 55 (2016) 4197–4211.
[43] I. Zaharieva, H. Dau, M. Haumann, Biochemistry 55 (2016) 6996–7004.
[44] N. Schuth, I. Zaharieva, P. Chernev, G. Berggren, M. Anderlund, S. Styring, H. Dau, M. Haumann, Inorg. Chem. 57 (2018) 10424–10430.
[45] V. Krewald, M. Retegan, N. Cox, J. Messinger, W. Lubitz, S. DeBeer, F. Neese, D.A. Pantazis, Chem. Sci. 6 (2015) 1676–1695.
[46] V. Krewald, F. Neese, D.A. Pantazis, Isr. J. Chem. 55 (2015) 1219–1232.
[47] N. Cox, M. Retegan, F. Neese, D.A. Pantazis, A. Boussac, W. Lubitz, Science 345 (2014) 804–808.
[48] A. Boussac, A.W. Rutherford, M. Sugiura, Biochim. Biophys. Acta Bioenerg. 1847 (2015) 576–586.
[49] Y. Sanakis, N. Ioannidis, G. Sioros, V. Petrouleas, J. Am. Chem. Soc. 123 (2001) 10766–10767.
[50] N. Ioannidis, J.H.A. Nugent, V. Petrouleas, Biochemistry 41 (2002) 9589–9600.
[51] N. Ioannidis, V. Petrouleas, Biochemistry 39 (2000) 5246–5254.
[52] A. Boussac, M. Sugiura, Y. Inoue, A.W. Rutherford, Biochemistry 39 (2000) 13788–13799.
[53] I.D. Young, M. Ibrahim, R. Chatterjee, S. Gul, F.D. Fuller, S. Koroidov, A.S. Brewster, R. Tran, R. Alonso-Mori, T. Kroll, T. Michels-Clark, H. Laksmono, R.G. Sierra, C.A. Stan, R. Hussein, M. Zhang, L. Douthit, M. Kubin, C. de Lichtenberg, L. Vo Pham, H. Nilsson, M.H. Cheah, D. Shevela, C. Saracini, M.A. Bean, I. Seuffert, D. Sokaras, T.-C. Weng, E. Pastor, C. Weninger, T. Fransson, L. Lassalle, P. Bräuer, P. Aller, P.T. Docker, B. Andi, A.M. Orville, J.M. Glownia, S. Nelson, M. Sikorski, D. Zhu, M.S. Hunter, T.J. Lane, A. Aquila, J.E. Koglin, J. Robinson, M. Liang, S. Boutet, A.Y. Lyubimov, M. Uervirojnangkoorn, N.W. Moriarty, D. Liebschner, P.V. Afonine, D.G. Waterman, G. Evans, P. Wernet, H. Dobbek, W.I. Weis, A.T. Brunger, P.H. Zwart, P.D. Adams, A. Zouni, J. Messinger, U. Bergmann, N.K. Sauter, J. Kern, V.K. Yachandra, J. Yano, Nature 540 (2016) 453–457.
[54] C. Kupitz, S. Basu, I. Grotjohann, R. Fromme, N.A. Zatsepin, K.N. Rendek, M.S. Hunter, R.L. Shoeman, T.A. White, D. Wang, D. James, J.-H. Yang, D.E. Cobb, B. Reeder, R.G. Sierra, H. Liu, A. Barty, A.L. Aquila, D. Deponte, R.A. Kirian, S. Bari, J.J. Bergkamp, K.R. Beyerlein, M.J. Bogan, C. Caleman, T.-C. Chao, C.E. Conrad, K.M. Davis, H. Fleckenstein, L. Galli, S.P. Hau-Riege, S. Kassemeyer, H. Laksmono, M. Liang, L. Lomb, S. Marchesini, A.V. Martin, M. Messerschmidt, D. Milathianaki, K. Nass, A. Ros, S. Roy-Chowdhury, K. Schmidt, M. Seibert, J. Steinbrener, F. Stellato, L. Yan, C. Yoon, T.A. Moore, A.L. Moore, Y. Pushkar, G.J. Williams, S. Boutet, R.B. Doak, U. Weierstall, M. Frank, H.N. Chapman, J.C.H. Spence, P. Fromme, Nature 513 (2014) 261–265.
[55] M. Suga, F. Akita, M. Sugahara, M. Kubo, Y. Nakajima, T. Nakane, K. Yamashita, Y. Umena, M. Nakabayashi, T. Yamane, T. Nakano, M. Suzuki, T. Masuda, S. Inoue, T. Kimura, T. Nomura, S. Yonekura, L.-J. Yu, T. Sakamoto, T. Motomura, J.-H. Chen, Y. Kato, T. Noguchi, K. Tono, Y. Joti, T. Kameshima, T. Hatsui, E. Nango, R. Tanaka, H. Naitow, Y. Matsuura, A. Yamashita, M. Yamamoto, O. Nureki, M. Yabashi, T. Ishikawa, S. Iwata, J.-R. Shen, Nature 543 (2017) 131–135.
[56] J. Kern, R. Chatterjee, I.D. Young, F.D. Fuller, L. Lassalle, M. Ibrahim, S. Gul, T. Fransson, A.S. Brewster, R. Alonso-Mori, R. Hussein, M. Zhang, L. Douthit, C. de Lichtenberg, M.H. Cheah, D. Shevela, J. Wersig, I. Seuffert, D. Sokaras, E. Pastor, C. Weninger, T. Kroll, R.G. Sierra, P. Aller, A. Butryn, A.M. Orville, M. Liang, A. Batyuk, J.E. Koglin, S. Carbajo, S. Boutet, N.W. Moriarty, J.M. Holton, H. Dobbek, P.D. Adams, U. Bergmann, N.K. Sauter, A. Zouni, J. Messinger, J. Yano, V.K. Yachandra, Nature 563 (2018) 421–425.
[57] D.A. Pantazis, Inorganics 7 (2019) 55.
[58] J. Wang, M. Askerka, G.W. Brudvig, V.S. Batista, ACS Energy Letters 2 (2017) 2299–2306.
[59] M. Retegan, V. Krewald, F. Mamedov, F. Neese, W. Lubitz, N. Cox, D.A. Pantazis, Chem. Sci. 7 (2016) 72–84.
[60] M. Capone, D. Bovi, D. Narzi, L. Guidoni, Biochemistry 54 (2015) 6439–6442.
[61] M. Shoji, H. Isobe, K. Yamaguchi, Chem. Phys. Lett. 636 (2015) 172–179.
[62] H. Isobe, M. Shoji, J.-R. Shen, K. Yamaguchi, Inorg. Chem. 55 (2016) 502–511.
[63] Y. Pushkar, K.M. Davis, M.C. Palenik, J. Phys. Chem. Lett. 9 (2018) 3525–3531.
[64] T.A. Corry, P.J. O'Malley, J. Phys. Chem. Lett. 9 (2018) 6269–6274.
[65] H. Isobe, M. Shoji, T. Suzuki, J.-R. Shen, K. Yamaguchi, J. Chem. Theory Comput. 15 (2019) 2375–2391.
[66] P.E.M. Siegbahn, Phys. Chem. Chem. Phys. 14 (2012) 4849–4856.
[67] I. Ugur, A.W. Rutherford, V.R.I. Kaila, Biochim. Biophys. Acta Bioenerg. 1857 (2016) 740–748.
[68] A. Boussac, M. Sugiura, A.W. Rutherford, P. Dorlet, J. Am. Chem. Soc. 131 (2009) 5050–5051.
[69] X. Li, P.E.M. Siegbahn, U. Ryde, Proc. Natl. Acad. Sci. U. S. A. 112 (2015) 3979–3984.
[70] M. Askerka, J. Wang, D.J. Vinyard, G.W. Brudvig, V.S. Batista, Biochemistry 55 (2016) 981–984.
[71] M. Retegan, D.A. Pantazis, Chem. Sci. 7 (2016) 6463–6476.
[72] M. Retegan, D.A. Pantazis, J. Am. Chem. Soc. 139 (2017) 14340–14343.
[73] M. Pérez Navarro, W.M. Ames, H. Nilsson, T. Lohmiller, D.A. Pantazis, L. Rapatskiy, M.M. Nowaczyk, F. Neese, A. Boussac, J. Messinger, W. Lubitz, N. Cox, Proc. Natl. Acad. Sci. U. S. A. 110 (2013) 15561–15566.
[74] M. Retegan, F. Neese, D.A. Pantazis, J. Chem. Theory Comput. 9 (2013) 3832–3842.
[75] F. Neese, WIREs Comput. Mol. Sci. 2 (2012) 73–78.
[76] V.N. Staroverov, G.E. Scuseria, J. Tao, J.P. Perdew, J. Chem. Phys. 119 (2003) 12129–12137.
[77] F. Neese, F. Wennmohs, A. Hansen, U. Becker, Chem. Phys. 356 (2009) 98–109.
[78] M. Bühl, H. Kabrede, J. Chem. Theory Comput. 2 (2006) 1282–1290.
[79] M. Bühl, C. Reimann, D.A. Pantazis, T. Bredow, F. Neese, J. Chem. Theory Comput. 4 (2008) 1449–1459.
[80] K.P. Jensen, Inorg. Chem. 47 (2008) 10357–10365.
[81] V. Krewald, D.A. Pantazis, Dalton Trans. 45 (2016) 18900–18908.
[82] V. Krewald, F. Neese, D.A. Pantazis, J. Am. Chem. Soc. 135 (2013) 5726–5739.
[83] D.A. Pantazis, M. Orio, T. Petrenko, S. Zein, E. Bill, W. Lubitz, J. Messinger, F. Neese, Chem.—Eur. J. 15 (2009) 5108–5123.
[84] M. Orio, D.A. Pantazis, T. Petrenko, F. Neese, Inorg. Chem. 48 (2009) 7251–7260.
[85] C. Baffert, M. Orio, D.A. Pantazis, C. Duboc, A.G. Blackman, G. Blondin, F. Neese, A. Deronzier, M.-N. Collomb, Inorg. Chem. 48 (2009) 10281–10288.
[86] M. Roemelt, V. Krewald, D.A. Pantazis, J. Chem. Theory Comput. 14 (2018) 166–179.
[87] D.A. Pantazis, Inorganics 7 (2019) 57.
[88] E. van Lenthe, E.J. Baerends, J.G. Snijders, J. Chem. Phys. 101 (1994) 9783–9792.
[89] E. van Lenthe, J.G. Snijders, E.J. Baerends, J. Chem. Phys. 105 (1996) 6505–6516.
[90] C. van Wüllen, J. Chem. Phys. 109 (1998) 392–399.
[91] D.A. Pantazis, X.Y. Chen, C.R. Landis, F. Neese, J. Chem. Theory Comput. 4 (2008) 908–919.
[92] A. Schäfer, C. Huber, R. Ahlrichs, J. Chem. Phys. 100 (1994) 5829–5835.
[93] F. Weigend, Phys. Chem. Chem. Phys. 8 (2006) 1057–1065.
[94] S. Grimme, S. Ehrlich, L. Goerigk, J. Comput. Chem. 32 (2011) 1456–1465.
[95] S. Grimme, J. Antony, S. Ehrlich, H. Krieg, J. Chem. Phys. 132 (2010) 154104.
[96] A. Klamt, D. Schüürman, J. Chem. Soc. Perkin Trans. (2) (1993) 799–805.
[97] F. Weigend, R. Ahlrichs, Phys. Chem. Chem. Phys. 7 (2005) 3297–3305.
[98] V. Krewald, B. Lassalle-Kaiser, T.T. Boron, C.J. Pollock, J. Kern, M.A. Beckwith, V.K. Yachandra, V.L. Pecoraro, J. Yano, F. Neese, S. DeBeer, Inorg. Chem. 52 (2013) 12904–12914.
[99] M. Roemelt, M.A. Beckwith, C. Duboc, M.-N. Collomb, F. Neese, S. DeBeer, Inorg. Chem. 51 (2012) 680–687.
[100] G. Zahariou, M. Chrysina, V. Petrouleas, N. Ioannidis, FEBS Lett. 588 (2014) 1827–1831.
[101] G. Zahariou, N. Ioannidis, Photosynth. Res. 130 (2016) 417–426.
[102] M. Chrysina, J.C. de Mendonça Silva, G. Zahariou, D.A. Pantazis, N. Ioannidis, J. Phys. Chem. B 123 (2019) 3068–3078.
[103] A. Klauss, T. Sikora, B. Süss, H. Dau, Biochim. Biophys. Acta Bioenerg. 1817 (2012) 1196–1207.
[104] A. Klauss, M. Haumann, H. Dau, J. Phys. Chem. B 119 (2015) 2677–2689.
[105] H. Nilsson, F. Rappaport, A. Boussac, J. Messinger, Nat. Commun. 5 (2014) 4305.
[106] K. Yamaguchi, Y. Takahara, T. Fueno, Ab-initio molecular orbital studies of structure and reactivity of transition metal-oxo compounds, in: V.H. Smith, Jr.H.F. Scheafer, IIIK. Morokuma (Eds.), Applied Quantum Chemistry, D. Reidel, Boston, 1986, pp. 155–184.
[107] P.E.M. Siegbahn, R.H. Crabtree, J. Am. Chem. Soc. 121 (1999) 117–127.
[108] P.E.M. Siegbahn, Chem.—Eur. J. 14 (2008) 8290–8302.
[109] R.H. Crabtree, Chem. Soc. Rev. 46 (2017) 1720–1729.
[110] R. Gupta, T. Taguchi, B. Lassalle-Kaiser, E.L. Bominaar, J. Yano, M.P. Hendrich, A.S. Borovik, Proc. Natl. Acad. Sci. U. S. A. 112 (2015) 5319–5324.
[111] T. Taguchi, K.L. Stone, R. Gupta, B. Kaiser-Lassalle, J. Yano, M.P. Hendrich, A.S. Borovik, Chem. Sci. 5 (2014) 3064–3071.
[112] A. Klauss, M. Haumann, H. Dau, Proc. Natl. Acad. Sci. U. S. A. 109 (2012) 16035–16040.
[113] M. Haumann, P. Liebisch, C. Müller, M. Barra, M. Grabolle, H. Dau, Science 310 (2005) 1019–1021.
[114] D.B. Rice, G.B. Wijeratne, T.A. Jackson, J. Biol. Inorg. Chem. 22 (2017) 1281–1293.
[115] J.A. Rees, V. Martin-Diaconescu, J.A. Kovacs, S. DeBeer, Inorg. Chem. 54 (2015) 6410–6422.
[116] W.J. Song, M.S. Seo, S. DeBeer George, T. Ohta, R. Song, M.J. Kang, T. Tosha, T. Kitagawa, E.I. Solomon, W. Nam, J. Am. Chem. Soc. 129 (2007) 1268–1277.
[117] T.C. Weng, W.Y. Hsieh, E.S. Uffelman, S.W. Gordon-Wylie, T.J. Collins, V.L. Pecoraro, J.E. Penner-Hahn, J. Am. Chem. Soc. 126 (2004) 8070–8071.
[118] J. Yano, J. Robblee, Y. Pushkar, M.A. Marcus, J. Bendix, J.M. Workman, T.J. Collins, E.I. Solomon, S. DeBeer George, V.K. Yachandra, J. Am. Chem. Soc. 129 (2007) 12989–13000.
[119] D.F. Leto, T.A. Jackson, Inorg. Chem. 53 (2014) 6179–6194.
[120] B. Lassalle-Kaiser, C. Hureau, D.A. Pantazis, Y. Pushkar, R. Guillot, V.K. Yachandra, J. Yano, F. Neese, E. Anxolabéhère-Mallart, Energy Environ. Sci. 3 (2010) 924–938.
[121] L.I. Krishtalik, Biochim. Biophys. Acta Bioenerg. 849 (1986) 162–171.
[122] N. Cox, J. Messinger, Biochim. Biophys. Acta Bioenerg. 1827 (2013) 1020–1030.
[123] M. Shoji, H. Isobe, Y. Shigeta, T. Nakajima, K. Yamaguchi, J. Phys. Chem. B 122 (2018) 6491–6502.
[124] T. Lohmiller, V. Krewald, A. Sedoud, A.W. Rutherford, F. Neese, W. Lubitz, D.A. Pantazis, N. Cox, J. Am. Chem. Soc. 139 (2017) 14412–14424.